In-vivo assessment of microvascular functional dynamics by combination of cmOCT and wavelet transform

Smirni, Salvatore; MacDonald, Michael P.; Robertson, Catherine P.; McNamara, Paul M.; O'Gorman, Sean; Leahy, Martin J.

Published in:
Dynamics and Fluctuations in Biomedical Photonics XV

DOI:
10.1117/12.2289814

Publication date:
2018

Document Version
Peer reviewed version

In-vivo assessment of microvascular functional dynamics by combination of cmOCT and wavelet transform

Salvatore Smirni[1], Michael P. MacDonald[1,2], Catherine P. Robertson[1], Paul M. McNamara[3], Sean O'Gorman[3], Martin J. Leahy[3,4] and Faisel Khan[1]

[1]School of Medicine, Ninewells Hospital, University of Dundee, Dundee, DD1 9SY, UK
[2]School of Science and Engineering, University of Dundee, Nethergate, Dundee, DD1 4HN, UK
[3]Tissue Optics and Microcirculation Imaging facility, National University of Ireland, Galway
[4]Royal College of Surgeons (RCSI), Dublin, Ireland

ABSTRACT

The cutaneous microcirculation represents an index of the health status of the cardiovascular system. Conventional methods to evaluate skin microvascular function are based on measuring blood flow by laser Doppler in combination with reactive tests such as post-occlusive reactive hyperaemia (PORH). Moreover, the spectral analysis of blood flow signals by continuous wavelet transform (CWT) reveals nonlinear oscillations reflecting the functionality of microvascular biological factors, e.g. endothelial cells (ECs). Correlation mapping optical coherence tomography (cmOCT) has been previously described as an efficient methodology for the morphological visualisation of cutaneous micro-vessels. Here, we show that cmOCT flow maps can also provide information on the functional components of the microcirculation. A spectral domain optical coherence tomography (SD-OCT) imaging system was used to acquire 90 sequential 3D OCT volumes from the forearm of a volunteer, while challenging the micro-vessels with a PORH test. The volumes were sampled in a temporal window of 25 minutes, and were processed by cmOCT to obtain flow maps at different tissue depths. The images clearly show changes of flow in response to the applied stimulus. Furthermore, a blood flow signal was reconstructed from cmOCT maps intensities to investigate the microvascular nonlinear dynamics by CWT. The analysis revealed oscillations changing in response to PORH, associated with the activity of ECs and the sympathetic innervation. The results demonstrate that cmOCT may be potentially used as diagnostic tool for the assessment of microvascular function, with the advantage of also providing spatial resolution and structural information compared to the traditional laser Doppler techniques.

Keywords: microcirculation imaging; cmOCT; continuous wavelet transform; nonlinear dynamics; cardiovascular risk;

1. INTRODUCTION

1.1 Cutaneous microcirculation for the assessment of cardiovascular risk

The microcirculation is a network of tiny blood vessels distributed in all the tissues of the body, which ensure the normal perfusion of the organs, the maintenance of a normal blood pressure, and the exchange of nutritive substances and waste metabolites between blood and tissue[1,2]. Microvascular dysfunction is involved in the development of several diseases, such as cardiovascular complications of diabetes, cardiomyopathy, and hypertension[1]. Therefore, the evaluation of the microcirculation is a powerful modality for the assessment of cardiovascular disease (CVD) risk, which could find potential diagnostic applications[1]. Nonetheless, the examination of microvascular function *in-vivo* relies on invasive techniques such as coronary angiography[1]. This problem may be addressed by using non-invasive methodologies for the *in-vivo* examination of microcirculation from peripheral organs, i.e. skin[1,3,4]. Indeed, several studies have demonstrated that skin microcirculation reflects the health status of the coronary microvasculature[4], and could be used as biomarker of CVD risk. For this reason, over the past number of years, many non-invasive technologies have been developed for either the evaluation of skin microvascular function or the imaging of skin microvascular structure.

1.2 Examination of cutaneous microvascular function by Laser Doppler and LSCI

The conventional methods for the evaluation of skin microvascular function are laser Doppler or laser speckle contrast imaging (LSCI) in combination with functional tasks, e.g. post-occlusive reactive hyperaemia (PORH). Laser Doppler techniques are generally classified in laser Doppler flowmetry (LDF) and laser Doppler imaging (LDI), based on sensing the Doppler shift of red or infrared light backscattered by moving red blood cells (RBCs) for the calculation of the mean blood perfusion in small tissue areas[2,3,5,6]. LDF allows the continuous measurement of blood flow by a single-point laser probe in direct contact with the cutaneous tissue[5]. The application of spectral analytical methods, i.e. the continuous wavelet transform (CWT), on LDF time series is powerful to investigate the nonlinear dynamics of blood flow providing information on the function of biological microvascular factors, such as endothelial cells (ECs), vascular smooth muscle cells (VSMCs), and the microvascular sympathetic nerves[7,8]. Nonetheless, LDF has low reproducibility because of the heterogeneous structure of skin compared to the small area analysed by the single-point probe[2,3,5,6]. This shortcoming is addressed by LDI, a contactless method that employs a laser placed at a distance above the skin to generate two-dimensional perfusion maps covering a larger skin region[3,5,6]. However, LDI cannot be used for the study of flow nonlinear fluctuations due to the slow sampling frequency of discrete perfusion maps during the measurements[3]. LSCI is a contactless technique based on sensing the reduction of the speckle contrast pattern caused by moving RBCs when a laser beam hits the skin, for estimating a perfusion value proportional to RBCs velocity[5,6]. The advantage of LSCI is providing both temporal and spatial resolution, however the method has low penetration depth compared to laser Doppler, and is highly sensitive to movement artefacts[5,6]. Furthermore, both of laser Doppler and LSCI do not allow the visualisation of micro-vessels[2,5,6]. Laser Doppler and LSCI blood flow data are expressed in perfusion arbitrary units (PU), making it necessary the combination of measurements with reactive tasks for assessing the relative changes of flow while challenging blood vessels with a variety of stimuli[5,6]. An example of functional task is PORH, based on monitoring the blood perfusion increase induced by a temporary period of ischaemia obtained through the occlusion of flow in the brachial artery[5,6]. The occlusion is performed by using a pressure cuff placed on the upper part of the tested arm, and the microcirculation is generally monitored from the volar forearm or the fingertips[5,6].

1.3 Methods for the imaging of skin micro-vessels

The cutaneous micro-vessels can be imaged *in-vivo* by a variety of techniques based on optical microscopy, 3D photoacoustic imaging or optical coherence tomography (OCT). The optical microscopy methods, i.e. capillaroscopy, orthogonal polarisation spectral imaging (OPS) and sidestream dark-field imaging (SDF), are based on the use of a microscope provided with a light source (white or green polarised light) for the transmission of images to a videocamera[2,6]. Capillaroscopy allows mainly the imaging of the structural organisation of capillaries in skin sites with thinner epithelium (i.e. the nailfold)[2,9]. This method is limited by the generation of low-contrast images[6] and the requirement of invasive fluorescent dyes to visualise blood vessels from thicker skin regions[2,6]. OPS and SDF provide better resolution images than capillaroscopy thanks to the use of non-invasive green polarised light[2,10]. However, both the techniques are sensitive to motion and pressure artefacts[6] and the imaging is optimal only for thinner cutaneous areas, e.g. the sublingual tissue[2]. All the optical microscopy methods provide two-dimensional images with ambiguous depth resolution leading to the impossibility of establishing the exact origin of the imaged microvascular layer[9,11]. This shortcoming has been solved by the implementation of techniques for the three-dimensional imaging of the microcirculation, such as 3D photoacoustic imaging and OCT[9,11]. The 3D photoacoustic imaging is a full light penetration depth method[12], employing low scattering ultrasound waves generated in all the directions by a pulsed laser light and absorbed by haemoglobin and melanin in the skin to provide contrast agents for the imaging of blood vessels[9,13,14]. Although photoacoustic imaging provides a full light penetration depth, the technique is characterised by low spatial resolution associated with the detection of ultrasound waves leading to poor structural images[9]. The development of photoacoustic microscopy (PAM) and optical resolution photoacoustic microscopy (OR-PAM) has allowed addressing the problem providing high-resolution images, even though this is still restricted to superficial capillaries[9]. Furthermore, photoacoustic imaging is limited by the use of a coupling medium at direct contact with the skin, which can affect the microcirculation and false the results[9]. OCT is a non-invasive method that uses a broadband near infrared light source placed at a distance above the skin to generate a low coherence gate for the selection of backscattered light from different tissue depths, providing two-dimensional and three-dimensional *in-vivo* morphological images[15]. OCT allows overcoming some shortcomings of photoacoustic imaging, by providing cross-sectional images comparable to conventional optical biopsies with high structural resolution in the order of micrometers[16,17]. However, OCT suffers of poor penetration depth compared to photoacoustic imaging[18].

1.4 Simultaneous assessment of microcirculation morphology and function

The advantage of laser Doppler and LSCI compared to the techniques for the visualisation of micro-vessels is the possibility to detect functional information that may be used for diagnostic purposes. Indeed, microvascular dysfunction is an early factor preceding the morphological damage to micro-vessels, which characterises the initial stages of cardiovascular pathologies[1,3]. However, LDI and LSCI are not suitable for a complete evaluation of the microcirculation because they do not allow micro-vessels visualisation and are characterised by uncertain spatial and depth resolution. For these reasons, many methods for the morphological imaging of the microcirculation have been implemented further to allow the simultaneous assessment of microvascular function and structure. For example, photoacoustic imaging may provide functional information associated to the oxygenation of the examined microvascular area, by tracing the light absorbed by haemoglobin at different wavelengths[19]. Additional examples are the improvements of OCT, adding contrast mechanisms based on the Doppler shift (DOCT)[20] and the speckle variance (svOCT)[21] principles to image blood flow, or by the development of data processing methods based on the discrimination of static and flow dynamic regions of the skin, i.e. Doppler optical micro-angiography (DOMAG)[22]. Nonetheless, the mentioned methods are not optimal for different reasons, such as angular dependence of the acquisitions leading to the production of incomplete flow maps (DOCT)[9,11], requirement of previous knowledge of the morphology to trace blood flow (svOCT)[9], and long post-processing time required for obtaining blood flow maps (DOMAG)[9]. To address these shortcomings, recently a novel technique for the *in-vivo* visualisation of micro-vessels named correlation mapping OCT (cmOCT) has been developed, which provides high-resolution structural maps of the microcirculation with potential to gain also functional information[9,11]. The technique is based on correlation coefficient statistics to detect blood flow from the OCT signal[9,11], by discriminating the moving scatters characterising the cutaneous areas containing active blood vessels and the stationary scatters in the skin locations lacking of blood vessels[9,11]. This is achieved by performing the cross-correlation analysis between adjacent two-dimensional B-frames of an OCT volume sampled from the skin, which returns high correlation coefficients for the static areas similar between different B-frames, and low correlation coefficients for the microvascular areas characterised by the presence of blood flow[9,11]. The correlation map generated from the analysis reveals the location of blood flow allowing the visualisation of the micro-vessels[9,11]. The benefits of cmOCT are the apparent angle independence of the method[11], the fact that it is not required the previous knowledge of the microvascular morphology to determine blood flow areas, and fast data processing to generate the flow maps[9].

1.5 Goal and findings of the research

Despite the suitability of cmOCT for the imaging of microvascular structure has been demonstrated[9,11], less proof is reported about the use of this method for the study of microvascular function. In this work, we show that cmOCT can be applied successfully for the study of microvascular function. We demonstrate that collecting many sequential low-resolution 3D OCT volumes from the human forearm during PORH functional task and processing the volumes by cmOCT it is possible to generate sequential blood flow maps at several tissue depths clearly tracing the temporal changes of flow typical of PORH test. Furthermore, the intensity of cmOCT flow maps was used to reconstruct a continuous time series for the study of blood flow nonlinear fluctuations by the application of the CWT spectral analysis. The wavelet examination of the reconstructed signal revealed blood flow oscillations associated with the physiological activity of biological factors playing a fundamental role in microvascular function: oscillations related to endothelial vasodilatory mechanisms mediated by ECs, and the neurogenic oscillation that reflects the contribution of the microvascular sympathetic nerves to vasomotion. The CWT oscillators displayed changes in their spectral energy during reactive hyperaemia similar to those described in literature for the LDF signal. Therefore, our results demonstrate that cmOCT is suitable for the simultaneous evaluation of microcirculation structure and function. Next step will be the application of the technique to a larger number of subjects for testing the reproducibility of cmOCT and its applicability to clinical studies.

2. METHODS

2.1 Images acquisition

Data were collected from the volar forearm of a healthy woman aged 28, which signed an informed consent form. The experiment was performed in a laboratory room with controlled temperature (20 ± 1 °C), allowing 15-20 min of acclimatisation of the subject. The scans were obtained from the left volar forearm while the volunteer was laying in a clinical bed. The tested arm was fixed by employing a house-designed soft support to ensure a static and comfortable position during the examination preventing motion artefacts. The location for the acquisitions was selected avoiding hairy and injured areas. A pressure cuff was fixed in the upper part of the arm for performing a PORH functional test during the acquisition of the images. PORH response was induced by blocking blood flow through the brachial artery by applying a

pressure of 200 mmHg. A spectral domain (SD) OCT device (TEL2200C1, Thorlabs Inc., USA) was employed for imaging three-dimensional skin volumes. The system is provided with a superluminescent diode (SLD) with a center wavelength of 1300 nm, supporting a maximum imaging depth of 3.5 mm in non-scattering samples, an axial acquisition rate between 5.5 and 76 kHz, and an axial resolution of 5.5 µm in non-scattering samples. The sample arm contains a LSM003 (Thorlabs Inc., USA) scanning lens supporting a transverse resolution of 13 µm in air. An initial volume of 1.50 x 1.50 x 1.82 mm^3 was sampled from the forearm at a speed of 48 kHz with a sampling density of 1024 (length) x 1024 (width) x 512 (depth) pixels, to image the microvascular morphology of the examined location. The time employed for the acquisition of the structural volume was 50.9 s, which is too long for the evaluation of functional dynamics. Thus, the study of functional dynamics was performed by decreasing the scanning density to 256 x 256 x 512 pixels that can be acquired in ~6 s, allowing the fast collection of consecutive OCT volumes suitable for assessing microvascular function. Moreover, a fundamental requirement for visualising blood flow by cmOCT is a dense sampling below the lateral resolution of the consecutive 2D B-scans of the OCT volume, which guarantees a robust correlation between the motionless scatters of the adjacent B-scans. Thus, to ensure a spatial separation between the B-scans suitable for the cmOCT analysis the sampled area was reduced to 0.75 x 0.75 x 1 .82 mm^3, corresponding to a spatial separation of 2.9 µm. Although the possibility of acquiring each scan in ~6 s, the samples were collected at a rate of one volume every 16.6 s because the software associated with the OCT system (ThorImage OCT 4.3, Thorlabs Inc., USA) required around 10.6 s for saving each sample. In total, 90 consecutive low-resolution volumes were acquired from the forearm of the volunteer in a temporal period of ~25 min, while performing the PORH functional task. An initial 10 min collection of 36 OCT volumes was carried out to establish the blood flow at rest, then 18 volumes were collected for a 5 min occlusion period, and finally 36 volumes were collected for 10 min after the removal of the occlusion for tracking blood flow dynamic changes during PORH response.

2.2 cmOCT analysis

The cmOCT analysis to extract blood flow maps at different tissue depths from each OCT volume was carried out by using the Java algorithm implemented by Enfield *et al.*[9] and Jonathan *et al.*[11]. The algorithm is able to estimate the correlation coefficients between consecutive two-dimensional B-frames extracted from the OCT volume, by calculating the cross-correlation of a square grid from the first B-scan 1 (I_1) to the same grid from the adjacent B-scan 2 (I_2), as follow,

$$cmOCT(x,y) = \sum_{p=0}^{M} \sum_{q=0}^{N} \frac{\left[I_1(x+p,y+q)-\overline{I_1(x,y)}\right]\left[I_2(x+p,y+q)-\overline{I_2(x,y)}\right]}{\sqrt{\left(I_1(x+p,y+q)-\overline{I_1(x,y)}\right)^2\left(I_2(x+p,y+q)-\overline{I_2(x,y)}\right)^2}} \quad (1)$$

where M and N define the dimension of the grid, and $\bar{I}$ is the mean intensity of the grid. The grid is shifted along all the pixels of the B-frames to generate a 2D map with correlation coefficients between 0 and 1. The low correlation regions are displayed as bright areas representing blood flow, while the high correlation regions associated to the motionless scatters of the tissue are displayed as dark background areas of the map. A 7 × 7 kernel dimension of the grid was used to produce the cmOCT maps, which ensures a good sensitivity to blood flow without loss of spatial resolution due to kernal size. The maps were generated as maximum intensity projection (MIP) images, which allow a better visualisation of microvascular structure and the detection of the maximum flow intensity. To study micro-vessels from different cutaneous microvascular layers, the flow maps were produced from different depths of the OCT volumes, i.e. in the *en face* plane. This was achieved by determining the location of skin surface from the structural images, and employing the superficial region as a reference to determine the various depths of the underlying tissue. The typical anatomic morphology of cutaneous microcirculation was visualised, characterised by the presence of capillaries at a depth of 80-180 µm (dermal-epidermal junction) and horizontal micro-vessels at a depth of 300-400 µm (dermal plexus).

2.3 Reconstruction of blood flow time series

To test the suitability of cmOCT for the study of microvascular flow nonlinear dynamics by CWT spectral analysis, a continuous time series of blood flow was reconstructed from the cmOCT maps. First, the average image intensity was extracted by Matlab R2015a software from 90 sequential flow maps produced at the cutaneous depth of 300-400 µm during PORH test. Then, the intensity values were used as discrete data points to reconstruct a continuous signal, covering the 25 minutes time used in the experiment for collecting the volumes. The reconstruction was performed by piecewise cubic spline interpolation using Matlab R2015a, applying a temporal interval of 16.6 s between each pair of discrete data points that corresponds to the sampling frequency employed during the collection of the OCT volumes. The spline interpolation is a mathematical procedure to approximate a function by interpolating equally spaced discrete data points of the function. The technique uses a low-degree piecewise polynomial named spline, which reduces the interpolation error compared to

the normal polynomial interpolation. The method is advantageous for the approximation of a function over large intervals, which is not optimal by using a single polynomial that would require a large degree of the approximating polynomial introducing oscillatory artefacts (Runge's phenomenon) during the interpolation process. The spline interpolation addresses this problem by subdividing the interval [a,b] where the function *f* is continuous in smaller sub-intervals, and approximating *f* in every sub-interval by the use of low-degree polynomial pieces that define a composite spline function *s*. In this study, a third-degree cubic natural spline was used which allows the reconstruction of continuous processes reproducing the smooth curvature of the function to be approximated. As displayed by equation 2, the cubic spline function employs four terms to define a piecewise cubic polynomial between each pair of data points,

$$p_3(x) = ax^3 + bx^2 + cx + d\,, \tag{2}$$

where p_3 is the piecewise cubic polynomial, and a, b, c and d are the four coefficients defining p_3. The final curve is the result of the sum of many pieces reconstructed between each pair of data points. The reconstruction was carried out by employing the *cftool* instrument in Matlab R2015a, which allows performing the cubic spline interpolation by entering the vectors of time and experimental data points. Specifically, we have used a time vector of 90 time points defining an acquisition rate of each flow measurement every 16.6 s and a vector containing the 90 flow intensity values extracted from the sequential cmOCT maps. The values of the continuous signal obtained from the reconstruction were saved for the subsequent application of the CWT analysis. As discussed previously, a benefit of spline interpolation is that the approximation process does not produce oscillatory artefacts. Thus, applying this technique we have ensured that the results of the subsequent CWT analysis were representative of the real fluctuations of microvascular flow detected by cmOCT, without the effect of artefacts introduced during the reconstruction. However, a shortcoming of spline interpolation is the low accuracy in the reconstruction of the right and left ends of the function, due to the presence of a single known data point at each extremity. To prevent the generation of artefacts at the extremities of the reconstructed signal, the curve was broken off at the left and right tips ensuring that the beginning and termination of the signal were corresponding respectively to the initial and final experimental data points. Finally, it should be clarified that in this work, the spline interpolation was not employed as a numerical analysis to fit a model but the method was used as a technical procedure to obtain a continuous signal, which is a compulsory requirement to allow performing the CWT spectral analysis.

2.4 CWT spectral analysis

The continuous wavelet transform technique allows the study of microvascular flow nonlinear dynamics, revealing the contribution of specific components in the microcirculation (i.e. ECs, VSMCs, and sympathetic nerves) to the temporal dynamic changes of flow. The method is advantageous for the analysis of the oscillatory behaviour of signals showing heterogeneous oscillations over a large range of frequencies, e.g. the LDF signal, providing a good time-frequency resolution[7,8]. Here, the CWT was used for analysing the dynamic fluctuations of a blood flow signal reconstructed from the cmOCT maps generated at a skin tissue depth of 300-400 µm, to prove that cmOCT can provide functional microvascular information related to vasomotion. The method allowed the detection of fluctuations in the frequency ranges 21-52 x 10^{-3} Hz, 9.5-21 x 10^{-3} Hz and 5-9.5 x 10^{-3} Hz that respectively reflect the neurogenic activity of sympathetic nerves, the ECs activity nitric oxide (NO)-dependent, and the ECs activity NO-independent[8]. The myogenic oscillation related to VSMCs function was not detected because the OCT volumes were sampled at a frequency of each volume every 16.6 s, restricting the study to fluctuations up to ~60 x 10^{-3} Hz that is not enough to cover the entire myogenic frequency range located between 52-145 x 10^{-3} Hz [8]. The CWT analysis was implemented by using Matlab R2015a, according to the principles described by Stefanovska *et al.*[7,8]. The method is based on the employment of a set of non-orthogonal basic functions $\Psi_{s,t}$ providing a large frequency window scaled and shifted along the time domain for the extraction of the CWT ensuring an optimal time-frequency resolution[8]. The functions $\Psi_{s,t}$ for the calculation of the CWT of blood flow signals is obtained according to equation 3, by using a Morlet mother wavelet ψ scaled in the temporal domain by a factor s and a center time t, providing a window size suitable for the analysis of highly time-varying signals[8],

$$\Psi_{s,t}(u) = |s|^{-1/2}\ \psi\left(\frac{u-t}{s}\right), \tag{3}$$

where the Morlet mother wavelet ψ is estimated as displayed in equation 4 [8],

$$\psi(u) = \frac{1}{\sqrt{\pi}} e^{-iu} e^{-u^2/2}. \tag{4}$$

The CWT spectrum of a signal $g(u)$ is then extracted as shown in equation 5 [8],

$$\tilde{g}(s,t) = \int_{-\infty}^{\infty} \overline{\Psi}_{s,t}\ (u) g(u) du, \tag{5}$$

where $\overline{\Psi}$ is a complex conjugate of the basic window function removing any dependence of the technique from frequency scales, and $\tilde{g}(s,t)$ is the CWT spectral function defined by the scale s and time t [8]. The obtained CWT spectrum is characterised by a power/energy distributed at various frequencies, indicating the amount of signal located at specific frequencies at the time t. Explained in physiological terms, the CWT energy indicates the contribute of each microvascular oscillator (i.e. ECs) associated with a specific frequency range to blood flow changes at a precise time that for example may be the stage of a reactive test. Monitoring the changes of the CWT energy from specific frequency intervals allows the assessment of the function of specific microvascular components with potential clinical diagnostic applications.

3. RESULTS

3.1 Visualisation of skin microcirculation morphology

A first three-dimensional OCT volume was acquired from a 1.50 × 1.50 × 1.82 mm^3 area in the volar forearm of the volunteer to visualise the microcirculation morphology. The acquisition was performed in 50.9 s employing 1024 × 1024 A-scans, and the MIP flow maps were extracted at different tissue depths by cmOCT analysis. Figure 1 shows the structural *enface* MIPs at three different tissue depths obtained from the volunteer, displaying the classical cutaneous microvascular morphology described by Enfield *et al.*[9].

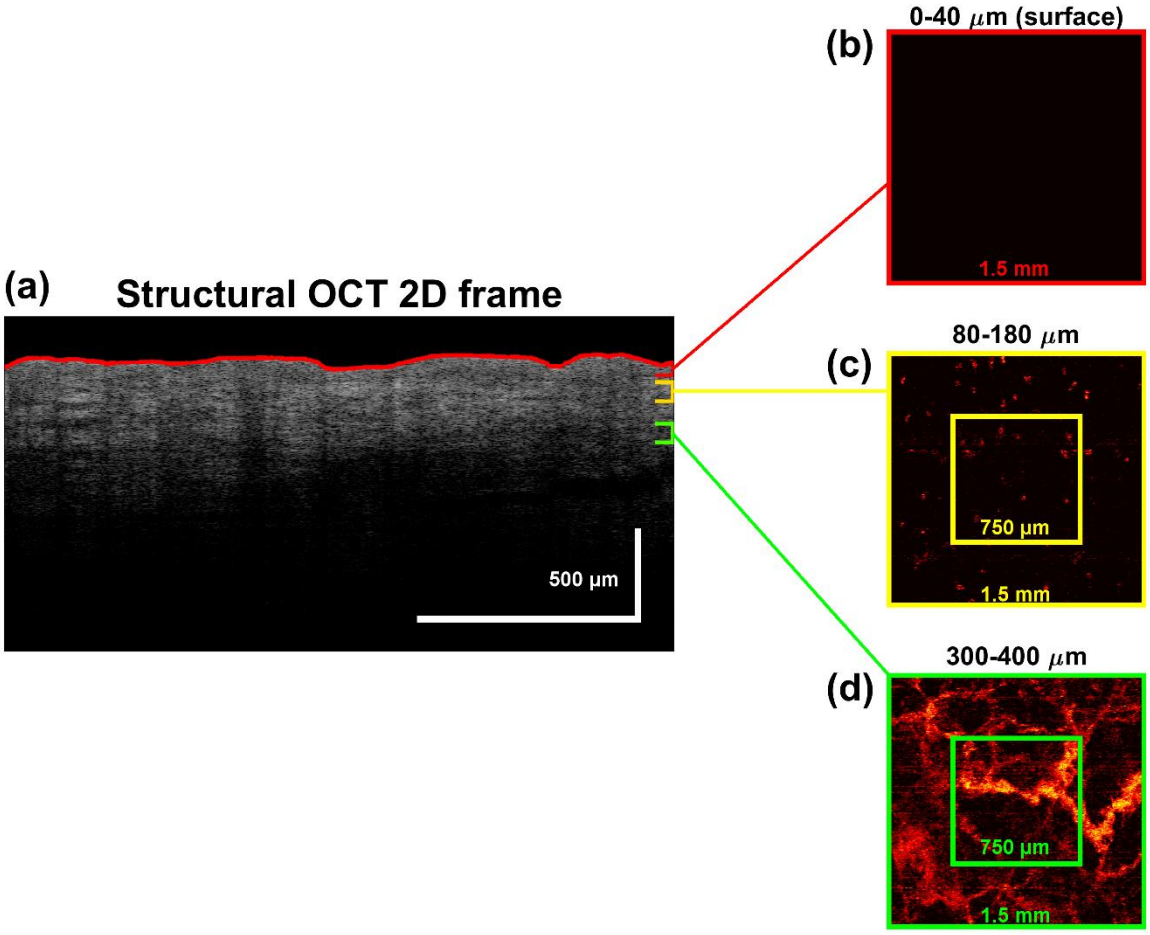

Figure 1 Morphological visualisation of skin micro-vessels from the forearm. (a) 2D structural B-scan from a 1.50 × 1.50 × 1.82 mm^3 OCT volume. The red area outlines the epidermis surface, the yellow region defines the dermal-epidermal junction, and the green area marks a part of the dermal plexus. **(b)** *Enface* 1.50 × 1.50 mm^2 MIP of the epidermis (0-40 µm). **(c)** *Enface* 1.50 × 1.50 mm^2 MIP of the dermal-epidermal junction (80-180 µm) where the capillaries are located. The smaller yellow square marks the 750 × 750 µm^2 region selected to study capillaries function. **(d)** *Enface* 1.50 × 1.50 mm^2 MIP of the dermal plexus (300-400 µm) characterised by a horizontal network of micro-vessels. The smaller green square marks the 750 × 750 µm^2 area selected to study arterioles/venules function.

Figure 1 (a) shows a structural 2D B-frame of the OCT volume, displaying a longitudinal view of the locations from which the cmOCT maps were produced. Figure 1 (b) displays the MIP *enface* map from the epidermis (0-40 µm) that, as expected, was characterised by absence of micro-vessels. Figure 1 (c) shows the MIP generated from a depth of 80-180 µm (dermal-epidermal junction), displaying the presence of micro-vessels with vertical direction corresponding to the capillary loops originated from the ascending blood vessels of the dermal layer, and appearing as red points in a black background. Figure 1 (d) shows an *enface* MIP of the skin at a depth of 300-400 µm (dermal plexus), displaying a network of arterioles and venules orientated horizontally from which, respectively, the nutritive substances are transferred to the capillaries and the waste metabolites to the venous system. To study microvascular function from 80-180 µm and 300-400 µm tissue depths, an *enface* plane of 0.75 × 0.75 mm^2 was selected from the structural images to perform sequential temporal acquisitions of 3D OCT volumes during reactive hyperaemia task. Figure 1 (c) and (d) illustrate the 750 × 750 μm^2 areas selected for monitoring capillaries and arterioles/venules functional dynamics, respectively marked by yellow and green squares.

3.2 Examination of blood flow functional dynamics from cmOCT maps

Ninety low-resolution volumes of the 0.75 × 0.75 × 1.82 mm^3 yellow/green regions shown in Figure 1 (c-d) were collected from the forearm of the volunteer during a 25 min PORH test, sampling each volume every 16.6 s. First, 36 samples were collected during a 10 min resting period, then 18 samples were acquired during a 5 min occlusion of blood flow, and finally 36 samples were collected in a 10 min period after the removal of the occlusion for monitoring flow changes during PORH response. The volumes were processed by cmOCT to obtain consecutive flow maps at 80-180 µm and 300-400 µm cutaneous depths for tracing, respectively, the flow dynamics of capillaries (Figure 2) and arterioles/venules (Figure 3).

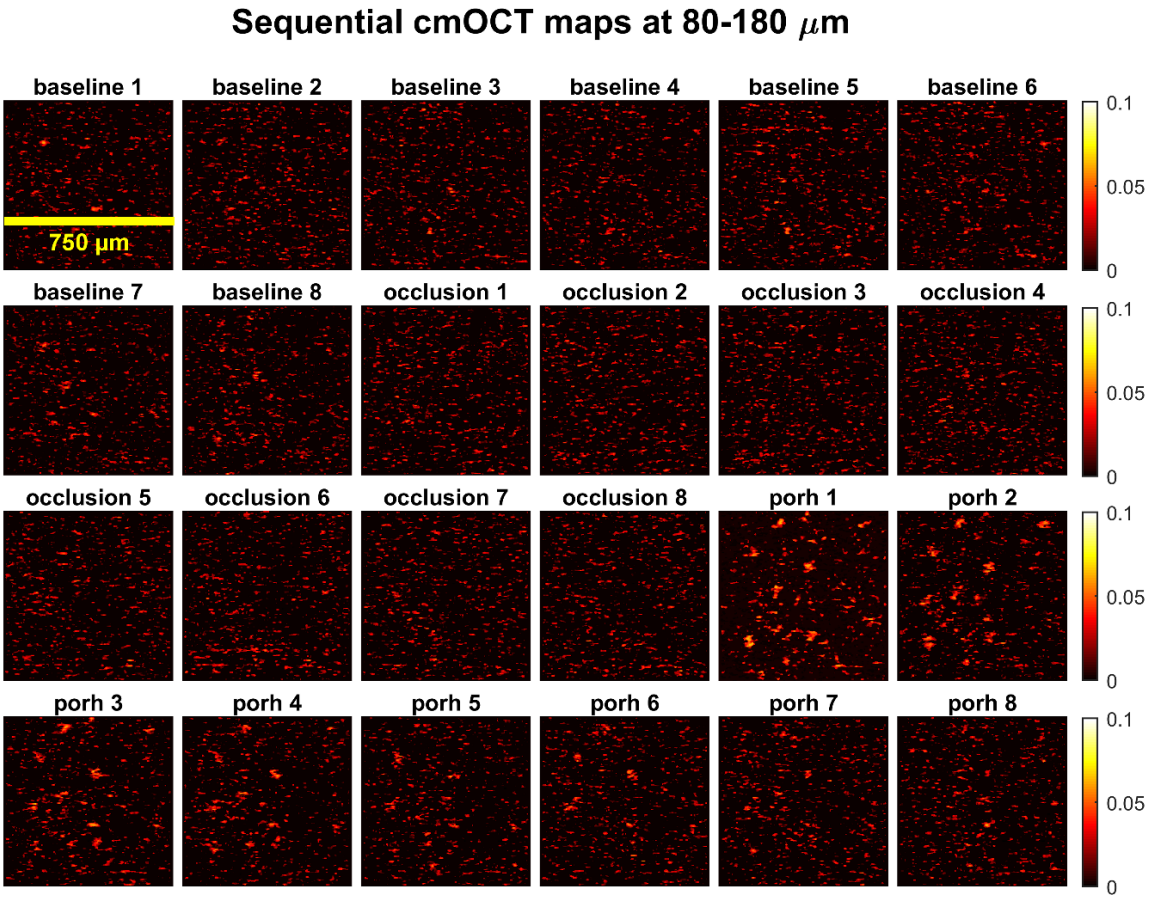

Figure 2 Consecutive cmOCT flow maps obtained at a depth of 80-180 µm from OCT volumes collected during PORH task. Temporal *enface* MIPs from the 750 × 750 μm^2 yellow region marked in Figure 1 (c) for the examination of capillaries microvascular function. The MIPs were generated from 0.75 × 0.75 × 1.82 mm^3 volumes collected every 16.6 s with a sampling density of 256 × 256 A-scans. The baseline 1-8 maps illustrate the flow detected at baseline before the application of the occlusion, the occlusion 1-4 and 5-8 maps correspond respectively to the flow detected after the beginning of the occlusion and before the end of the occlusion, and the porh 1-8 maps show the flow detected during the hyperaemic response.

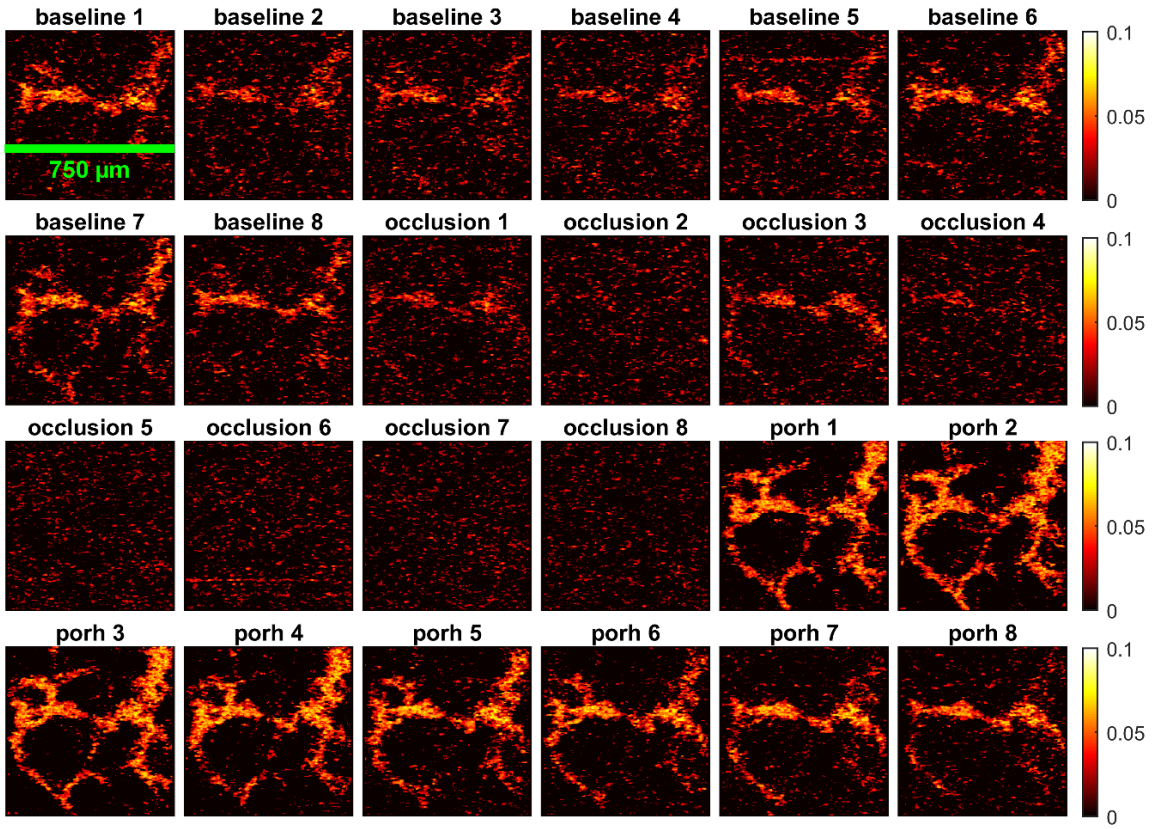

Figure 3 Consecutive cmOCT flow maps obtained at a depth of 300-400 µm from OCT volumes collected during PORH task. Temporal *enface* MIPs from the 750 × 750 µm^2 green region marked in Figure 1 (d) for the examination of arterioles/venules microvascular function. The MIPs were generated from 0.75 × 0.75 × 1.82 mm^3 volumes collected every 16.6 s with a sampling density of 256 × 256 A-scans. The baseline 1-8 maps illustrate the flow detected at baseline before the application of the occlusion, the occlusion 1-4 and 5-8 maps correspond respectively to the flow detected after the beginning of the occlusion and before the end of the occlusion, and the porh 1-8 maps show the flow detected during the hyperaemic response.

Figure 2 and Figure 3 display the *enface* MIPs obtained from 24 volumes of the total 90 temporal samples, which represent the most important stages of PORH test. Although the quality of the maps was not optimal compared to the morphological images, they clearly traced the flow changes typical of PORH reactive task. The capillaries did not show relevant flow changes during occlusion (Figure 2, occlusion 1-8) compared to the flow at rest (Figure 2, baseline 1-8), while the micro-vessels in the dermal plexus showed a relevant decrease and disappearance of flow during occlusion (Figure 3, occlusion 1-8) compared to the flow at rest (Figure 3, baseline 1-8). These findings may indicate the delivery of the residual blood flow from arterioles to capillaries during the occlusion period, ensuring the feeding of the epidermis during ischaemia. On the other hand, a relevant growth of the flow typical of the hyperaemic response was observed during PORH either for the capillaries or the dermal micro-vessels (Figures 2-3, porh 1-8), related to the vascular reactivity for the restoration of a normal blood flow after removal of the occlusion. These findings prove that cmOCT allows tracking the microcirculatory dynamics and may be used for the investigation of microvascular function.

3.3 Reconstruction of blood flow signal from cmOCT maps

To demonstrate further the applicability of cmOCT for the study of microvascular function, the cmOCT maps were employed for tracing the nonlinear dynamics of blood flow to detect the oscillatory activity of microvascular components contributing to the rhythmic vaso-relaxation induced by PORH stimulation. The task was achieved by reconstructing a continuous flow signal from the intensities of the sequential temporal cmOCT maps and processing the obtained time series by CWT spectral analysis. The reconstruction process was a fundamental step to allow performing the CWT analysis, which is a technique applicable only on continuous time-varying signals. Figure 4 shows the blood flow time series

obtained by using the mean intensity values extracted from the 90 sequential cmOCT maps generated at a depth of 300-400 µm as discrete data points to reconstruct a curve covering the 25 min period of the reactive test. The reconstruction was performed by piecewise cubic spline interpolation method that is advantageous because no oscillatory artefacts are introduced between each pair of discrete data points during the reconstruction process. The curve in Figure 4 clearly outlines the classic flow trend of the reactive hyperaemia task, showing a decrease of blood flow during the ischaemic period, and a relevant increase of flow during PORH vasodilation response up to a maximal peak before the gradual restoration of the baseline flow. This is a further proof that cmOCT is suitable for the study of functional dynamics.

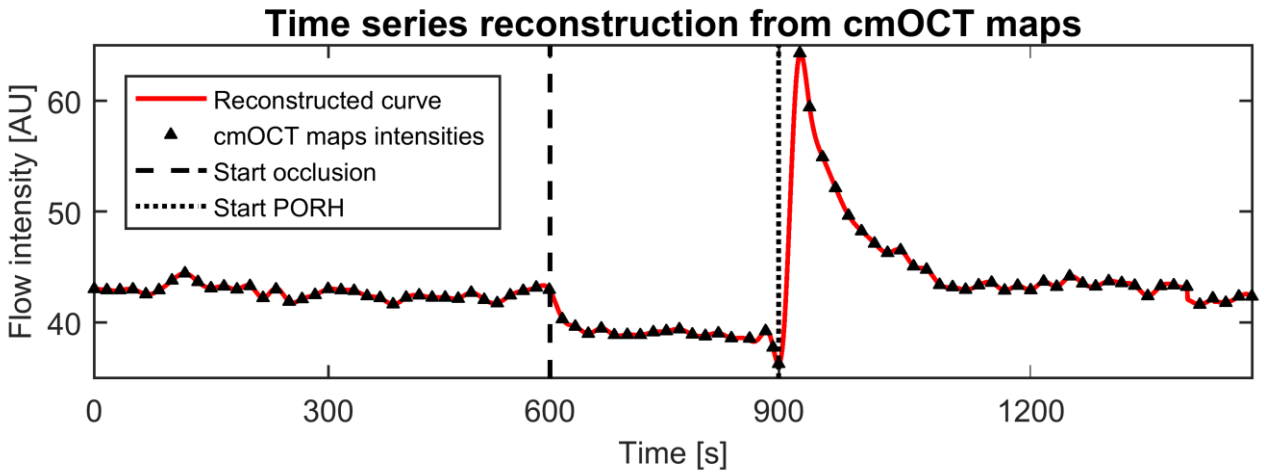

Figure 4 Reconstruction of a continuous blood flow signal from cmOCT maps. Blood flow curve reconstructed by piecewise cubic spline interpolation of the discrete average intensity values obtained from 90 sequential cmOCT maps produced at a cutaneous depth of 300-400 µm. A time interval of 16.6 s was applied between each pair of discrete data points to cover the 25 min period of the PORH functional task. The flow is expressed in arbitrary units (AU).

3.4 CWT spectral analysis of the blood flow signal reconstructed from cmOCT maps

The CWT analysis of the signal reconstructed from cmOCT maps revealed oscillations in the frequency ranges 21-52 x 10^{-3} Hz, 9.5-21 x 10^{-3} Hz and 5-9.5 x 10^{-3} Hz, which respectively reflect the neurogenic modulation of microvascular tone mediated by the sympathetic nerves, and the regulation of microvascular tone mediated by ECs through NO-dependent and NO-independent pathways[8]. Figure 5 displays the CWT analysis of the reconstructed flow signal shown in Figure 4. Figure 5 (a) displays the CWT scalogram chart that shows a gradient coloured map representing the distribution of the wavelet energy of the signal in the time-frequency domain. The dark blue regions represent the lowest energies and the dark red areas the highest energies. The chart clearly outlines the growth of energy during PORH response in all the identified oscillatory frequency intervals, reflecting the endothelial and sympathetic modulatory mechanisms activated during vasodilation. The time-averaged CWT spectrum in Figure 5 (b) distinguishes the maximum wavelet energy peaks at various frequency intervals corresponding to the specific microvascular oscillators (neurogenic, ECs NO-dependent, ECs NO-independent). This allows tracking the activity of each oscillator and making comparisons between different individuals, by extracting values of the maximal energy (amplitude), the overall energy (area under the curve), and the frequency from each wavelet peak during the different stages of PORH task. For example, in Figure 5 (b) an increase of the amplitude and energy of all the oscillators was clearly observed during PORH response (black line) compared to occlusion (red line) and baseline (blue line). These data are in agreement with the results reported for the spectral analysis of LDF signals measured during PORH functional test[23]. Indeed, the growth of energy reflects the vasodilation modulated by ECs, VSMCs and the neurogenic control to allow the reperfusion of the cutaneous tissue after an occlusion period. The CWT spectral analysis showed results in agreement with the current techniques for the examination of microvascular nonlinear fluctuations. Therefore, this is an additional evidence of the suitability of cmOCT for monitoring microvascular function.

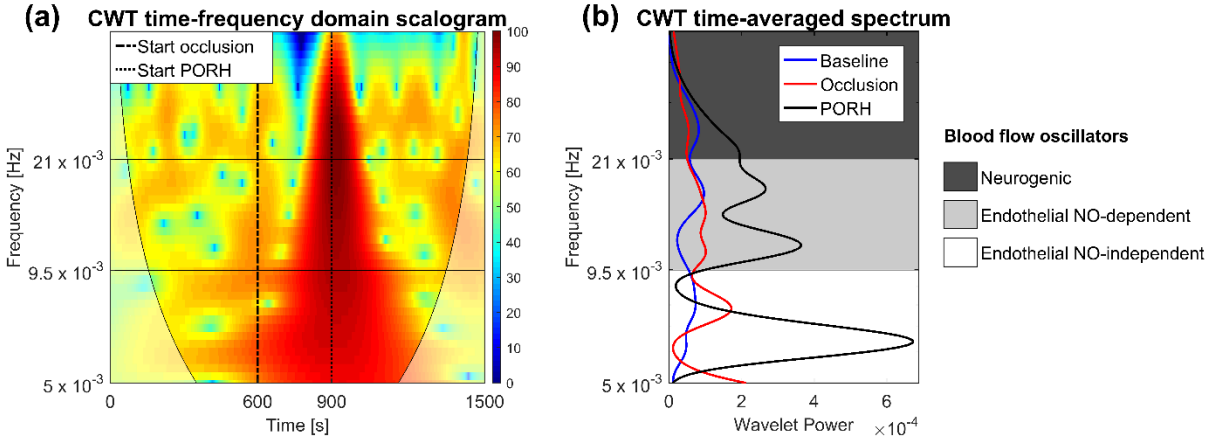

Figure 5 CWT spectral analysis of a blood flow signal reconstructed from cmOCT maps produced at a depth of 300-400 µm. **(a)** CWT scalogram displaying the distribution of the wavelet power in the time-frequency domain represented by a coloured gradient map ranging from dark blue (low power) to dark red (high power). The coloured areas in the scalogram are part of the "cone of influence", which is a time-frequency region where distortions of the wavelet transform due to the finite duration of the signal are irrelevant[24]. In contrast, the transparent regions in the corners at the bottom of the chart are regions outside of the cone in proximity of the time edges of the signal, where the CWT is characterised by boundary effects making the calculations from these areas uncertain[24]. **(b)** Time-averaged CWT spectra estimated for all the steps of PORH functional task. The graphs discriminate the CWT maximum amplitude peak and overall energy (area under the curve of the peak) related to each specific microvascular oscillator. The neurogenic (21-52 x 10^{-3} Hz), ECs NO-dependent (9.5-21 x 10^{-3} Hz), and ECs NO-independent (5-9.5 x 10^{-3} Hz) oscillators were detected.

4. DISCUSSION AND CONCLUSIONS

In this study, we have shown that cmOCT method allows the simultaneous imaging of skin microcirculation morphology and monitoring of microvascular function. Although the resolution of the functional temporal cmOCT maps was low, they allowed tracking the overall microvascular dynamics with spatial resolution at various tissue depths, showing results similar to those reported for the conventional techniques employed to study microvascular function (i.e. LDF). This is demonstrated by the blood flow trend typical of PORH reactive test observed on the cmOCT maps (Figures 2-3), and also reflected on the reconstructed flow signal displayed in Figure 4. Furthermore, additional evidence was provided by the identification of dynamic microvascular oscillators characterising the reconstructed signal associated with biological components in the microcirculation (Figure 5), which displayed trends of the wavelet spectral energy similar to those reported for the spectral analysis of LDF time series recorded during PORH test. The CWT analysis did not allow the detection of the myogenic oscillator related to the activity of VSMCs, which are implicated in the mechanical modification of micro-vessels diameter during vasomotion. This was due to the long time required by the ThorImage software (Thorlabs Inc., USA) for saving the OCT volumes during the acquisition of the images, allowing a scanning rate of one volume every 16.6 s that was not sufficient to detect the myogenic oscillation. The use of a more powerful computer in the future may help to improve the performance of the software, allowing a faster data storage to increase the sampling frequency and detect the myogenic oscillator. Overall, the findings from this study suggest that cmOCT may be used as a tool for the study of microvascular function with possible diagnostic applications. However, further experiments in a larger number of subjects are required to demonstrate the robustness of the method and the eligibililty for clinical studies. In addition, the combination of cmOCT with the CWT spectral analysis may find several applications. For example, this may help to establish the contribution of each microvascular bed to vasomotion and clarify which layer is more involved in cutaneous PORH response, by comparing the spectral analysis of cmOCT blood flow signals reconstructed from different skin tissue depths. Another application may be the examination of endothelial function for diagnostic purposes by comparing the endothelial wavelet energy between healthy individuals and patients affected by cardiovascular disease (CVD).

ACKNOWLEDGMENTS

The research leading to these results has received funding from the People Programme (Marie Curie Actions) of the European Union's Seventh Framework Programme (FP7/2007-2013) under REA grant agreement n° 608133. The experiments were performed at the Tissue Optics and Microcirculation Imaging facility of the National University of

Ireland, Galway (NUIG) that was involved as associated academic partner in the Marie Curie PHOQUS research programme co-ordinated by the University of Dundee (Scotland).

REFERENCES

[1] Gutterman, D. D., Chabowski, D. S., Kadlec, A. O., Durand, M. J., Freed, J. K., Aissa, K. A. and Beyer, A. M., "The Human Microcirculation – Regulation of Flow and Beyond", Circ. Res., 118(1), 157–172 (2016).

[2] den Uil, C. A., Klijn, E., Lagrand, W. K., Brugts, J. J., Ince, C., Spronk, P. E. and Simoons, M. L., "The microcirculation in health and critical disease", Prog. Cardiovasc. Dis., 51(2), 161-70 (2008).

[3] Turner, J., Belch, J. J. and Khan, F., "Current concepts in assessment of microvascular endothelial function using laser Doppler imaging and iontophoresis", Trends Cardiovasc. Med., 18(4), 109-16 (2008).

[4] Khan, F., Patterson, D., Belch, J. J., Hirata, K. and Lang, C. C., "Relationship between peripheral and coronary function using laser Doppler imaging and transthoracic echocardiography", Clin. Sci. (Lond.), 115(9), 295-300 (2008).

[5] Roustit, M. and Cracowski, J. L., "Assessment of endothelial and neurovascular function in human skin microcirculation", Trends Pharmacol. Sci., 34(7), 373-84 (2013).

[6] Roustit, M. and Cracowski, J. L., "Non-invasive assessment of skin microvascular function in humans: an insight into methods", Microcirculation, 19(1), 47-64 (2012).

[7] Stefanovska, A., Bračič, M. and Kvernmo, H. D. "Wavelet analysis of oscillations in the peripheral blood circulation measured by laser Doppler technique", IEEE Trans. Biomed. Eng., 46(10), 1230-9 (1999).

[8] Shiogai, Y., Stefanovska, A. and McClintock, P. V., "Nonlinear dynamics of cardiovascular ageing", Phys. Rep., 488(2-3), 51-110 (2010).

[9] Enfield, J., Jonathan, E. and Leahy, M., "In vivo imaging of the microcirculation of the volar forearm using correlation mapping optical coherence tomography (cmOCT)", Biomed. Opt. Express, 2(5), 1184-1193 (2011).

[10] Daly, S. M. and Leahy, M., "'Go with the flow': A review of methods and advancements in blood flow imaging", J. Biophotonics, 6(3), 217-255 (2013).

[11] Enock, J., Enfield, J. and Leahy, M. J., "Correlation mapping method for generating microcirculation morphology from optical coherence tomography (OCT) intensity images", J. Biophotonics, 4, 583-587 (2010).

[12] Wang, L. V., "Prospects of photoacoustic tomography", Med. Phys., 35(12), 5758 (2008).

[13] Xu, M. and Wang, L. V., "Time-Domain Reconstruction for Thermoacoustic Tomography in a Spherical Geometry", IEEE Trans. Med. Imaging, 21(7), 814-822 (2002).

[14] Wang, X., Xu, Y. and Xu, M., "Photoacoustic tomography of biological tissues with high cross-section resolution: Reconstruction and experiment", Med. Phys., 29, 2799 (2002).

[15] Podoleanu, A. G., "Optical coherence tomography", J. Microsc., 247, 209-219 (2012).

[16] Mogensens, M. and Jemec, G. B. E., “Diagnosis of Nonmelanoma Skin Cancer/Keratinocyte Carcinoma: A Review of Diagnostic Accuracy of Nonmelanoma Skin Cancer Diagnostic Tests and Technologies”, Dermatol. Surg., 33(10), 1158-1174 (2007).

[17] Drexler, W., Morgner, U., Kärtner, F. X., Pitris, C., Boppart, S. A., Li, X. D., Ippen, E. P. and Fujimoto, J. G., “In vivo ultrahigh-resolution optical coherence tomography”, Optics Letters, 24(17), 1221-1223 (1999).

[18] Fercher, A. F., Drexler, W., Hitzenberger, C. K. and Lasser, T., “Optical coherence tomography - principles and applications”, Rep. Progr. Phys., 66(2), 239-303 (2003).

[19] Zhang, H. F., Maslov, K., Stoica, G. and Wang, L. V., “Functional photoacoustic microscopy for high-resolution and noninvasive in vivo imaging”, Nature Biotechnology, 24(7), 848-851 (2006).

[20] Wang, X., Milner, T. and Nelson, J., “Characterization of fluid flow velocity by optical Doppler tomography”, Optics letters, 20(11), 1337-1339 (1995).

[21] Barton, J. and Stromski, S., “Flow measurement without phase information in optical coherence tomography images”, Optics Express, 13(14), 5234-5239 (2005).

[22] Wang, R. K., Jacques, S. L., Ma, Z., Hurst, S., Hanson, S. R. and Gruber, A., “Three dimensional optical angiography”, Optics Express, 15(7), 4083-4097 (2007).

[23] Rossi, M., Pistelli, F., Pesce, M., Aquilini, F., Franzoni, F., Santoro, G. and Carrozzi, L., “Impact of long-term exposure to cigarette smoking on skin microvascular function”, Microvasc. Res., 93, 46-51 (2014).

[24] Iatsenko, D., McClintock, P. V. E. and Stefanovska, A., “Linear and synchrosqueezed time-frequency representations revisited: Overview, standards of use, resolution, reconstruction, concentration, and algorithms”, Digital Signal Processing, 42, 1-26 (2015).